frontiers | Frontiers in Earth Science

TYPE Original Research
PUBLISHED 19 September 2022
DOI 10.3389/feart.2022.939375

OPEN ACCESS

EDITED BY
Liang Zhang,
China University of Geosciences, China

REVIEWED BY
Ahmed M. Eldosouky,
Suez University, Egypt
Sirui Wang,
China University of Geosciences, China

*CORRESPONDENCE
Zheng-Jiang Ding,
110357960@qq.com
Guan-Wen Gu,
sun_ggw@163.com

SPECIALTY SECTION
This article was submitted to Economic Geology, a section of the journal Frontiers in Earth Science

RECEIVED 09 May 2022
ACCEPTED 25 July 2022
PUBLISHED 19 September 2022

CITATION
Xu Z-H, Ding Z-J, Gu G-W, Jiang J-Y, Wang L and Niu X-G (2022), Deep exploration of Jiaodong type gold deposit, taking Shanhou gold deposit, southern part of Zhaoping fault as an example.
Front. Earth Sci. 10:939375.
doi: 10.3389/feart.2022.939375

Deep exploration of Jiaodong type gold deposit, taking Shanhou gold deposit, southern part of Zhaoping fault as an example

Zhi-He Xu[1,2,3,4], Zheng-Jiang Ding[2]*, Guan-Wen Gu[1,3]*, Ji-Yi Jiang[1,3], Li Wang[5] and Xing-Guo Niu[6]

[1]Institute of Disaster Prevention, Sanhe, China, [2]Shandong Provincial Engineering Laboratory of Application and Development of Big Data for Deep Gold Exploration, Weihai, China, [3]Hebei Key Laboratory of Earthquake Dynamics, Sanhe, China, [4]Engineering Research Center of Geothermal Resources Development Technology and Engineering, Ministry of Education, Jilin University, Changchun, China, [5]College of Earth Sciences, Jilin University, Changchun, China, [6]Inner Mongolia Non-ferrous Geological Mining Industry, Huhehaote, China

Crustal response induced by the subduction of Paleo-Pacific Plate, is crucial to study the metallogenic law and prediction of Jiaodong type gold deposit. Gold deposits are preferentially hosted in the lithospheric-scale second-order faults, which provide migration channels, mineralization corridors, and the physicochemical conditions. Super-large gold deposits in northwestern Jiaobei Terrane are generally controlled by regional linear faults, such as Sansandao, Jiaojia, Zhaoping and Qixia faults. However, Zhaoping fault is exposed sporadically (in Xiadian and Jiangjiayao gold deposits) beneath a thick cover of Quaternary basalts, which indicating that limited information can be obtained by traditional geological survey. In this study, high-precision geophysical surveys such as gravity and controlled source audio frequency magnetotellurics (CSAMT) are conducted in the Shanhou gold deposit, which hosted in southern part of Zhaoping fault. Three integrated geophysical profiles results further identified the spatial distribution of second-order oblique-slip faults of Zhaoping fault and established the relationships between brittle deformation and mineralization. The spatial variability of stratum (high density 2.82 g/cm^3 and intermediate to high specific resistivity 4000 Ω m), brittle-slip faults (intermediate density 2.73 g/cm^3 and low specific resistivity 200 Ω m) and magmatite (low density 2.57 g/cm^3 high specific resistivity 8000 Ω m) are identified by two inversion techniques, including the man-machine interactive inversion technology and nonlinear conjugate gradient technology. In addition, the geophysical inversion pseudo sections delicately portray a smooth-out waveform low specific resistivity anomaly, which strongly couples with the spatial ore-hosted locations and enrichment places. The gold mineralized alteration zones generally dips to southeast and the angle changing from 45° to 30°, which are strong coupling with the large-scale acid magmatic

intrusion and extensional tectonics occurred in the late Mesozoic. Finally, according to the deep prospecting prediction, a gold ore body with 10 m in thickness was revealed by drilling below the depth of 1,015 m, which is hosting in the brittle deformation of Zhaoping fracture zone.

KEYWORDS

deep exploration, decratonic gold deposit, subduction of Paleo-Pacific Plate, Jiaodong gold province, geophysical method, cratonic destruction

Introduction

Jiaodong type gold deposit, which is the primary type of gold endowment in the North China Craton (NCC), generally formed after prolonged stabilization of the craton (Zhu et al., 2011, 2015). This type deposit occurs under transpressinal condition from a transpressional to transtensional tectonic setting, which induced by Late Mesozoic breakoff of the subduction slab and rollback of the Paleo-Pacific Plate (Deng et al., 2015; Liang et al., 2019). The metallogenic law has an evidently relationship with the NNE-NE-trending oblique-slip faults (Li et al., 2012; Deng et al., 2020; Li et al., 2022). Generally, the formation of cratons remained stable in the early Precambrian and hardly triggered large-scale tectono-magmatic activities and gold mineralization (Groves and Bierlein, 2007). However, multi-disciplinary observations indicate that the lithosphere of NCC has experienced unsteady flow. Two important gold metallogenic belts (the East gold belt and the West gold belt, Figure 1) formed during the metasomatic transformation of mantle-derived fluids and magmatic activities (Li et al., 2012; Cai et al., 2018) (Figure 1).

The Jiaodong gold province, with more than 5000 t of proven gold resources, is considered as the only global district that preserved giant gold resources in the East gold belt (Zhu et al., 2011; Deng et al., 2020). The aim of early prospecting

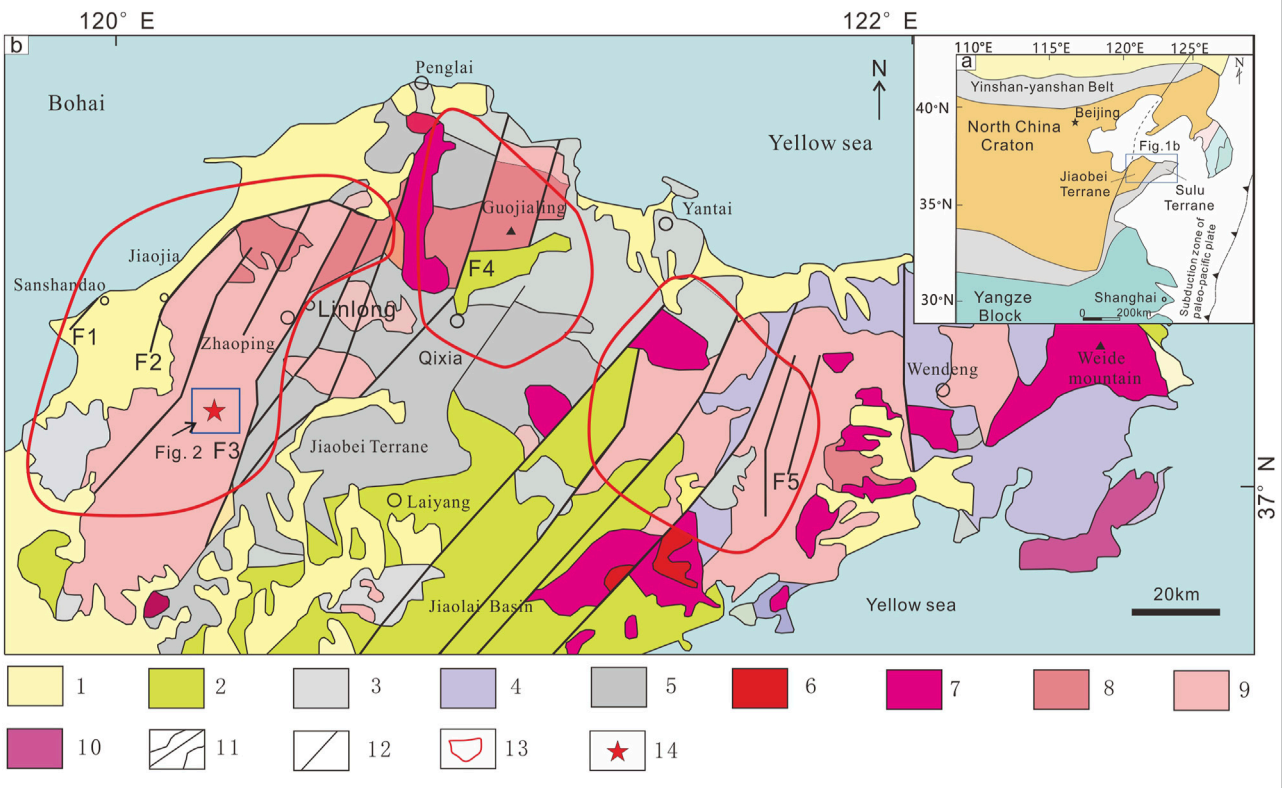

FIGURE 1
Simplified regional geological map, modified after Wu et al. (2022). **(A)** Simplified regional geological map of NCC; **(B)** Regional geological map of Jiaodong gold province. 1- Quaternary; 2- Mesozoic; 3- Proterozoic; 4- Neoproterozoic gneiss; 5- Archean greenstone belt; 6- Cretaceous Laoshan granite; 7- Cretaceous Weide mountain granite; 8- Cretaceous Guojialing granite; 9- Jurassic Linglong granite; 10- Triassic granite; 11- Geological boundary; 12- Fault; 13- Gold deposit accumulation region; 14- Laixi gold desposit; F1-Sanshandao fault; F2- Jiaojia fault; F3- Zhaoping fault; F4-Xilin-douya fault; F5-Jinniushan fault.

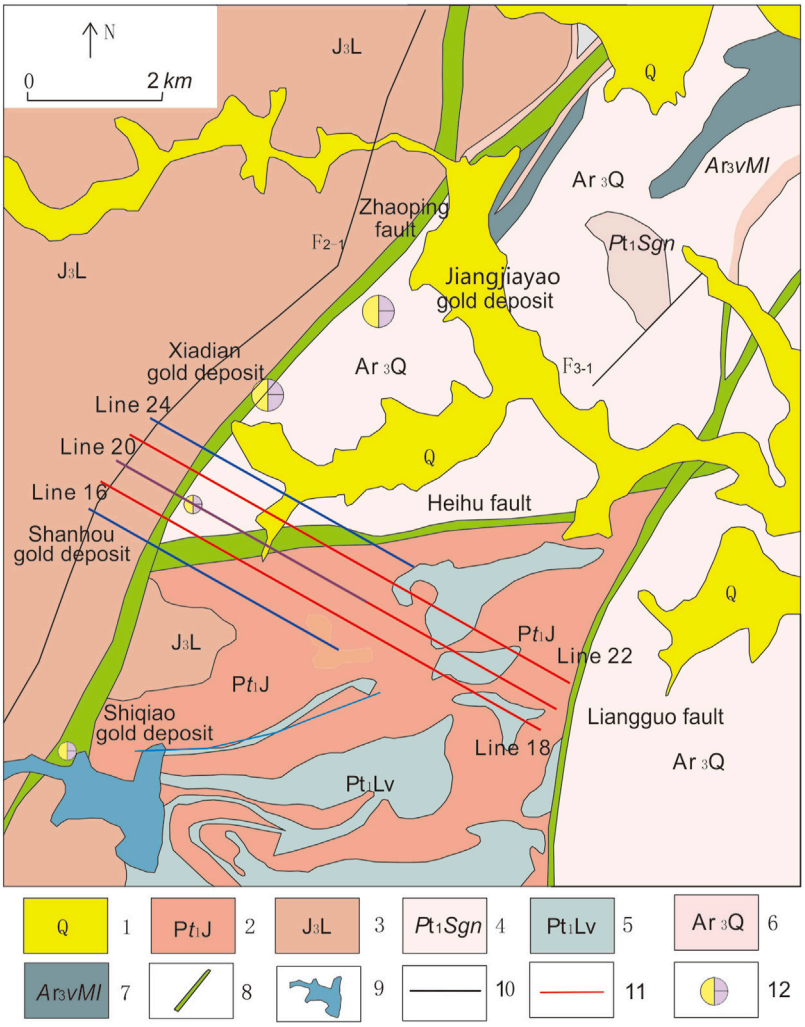

FIGURE 2
Simplified regional geological map of Shanhou gold deposit. 1- Quaternary; 2- Paleoproterozoic Jinshan Group; 3- Late Jurassic Linglong granite; 4- Paleoproterozoic Shuangdingshan gneiss; 5- Paleoproterozoic Penglai metabasite; 6- Archean Qixia gneiss; 7-Archean Luanjiazhai metabasite; 8- Deep-seated fault; 9-Reservoir; 10- Secondary fracture; 11- Geophysical profile; 12- Gold deposit.

direction is predominately the quartz vein type gold deposit and superficial prospecting. The proved gold reserves are only 340 t in the early stage of prospecting. As a result of the discovery of Jiaojia type gold deposit, geologists recognized that the regional faults not only created channels for transmitting ore, but also favored the occurrence space for mineralization (Groves et al., 2005, 2020; Zhang et al., 2020). Therefore, based on above metallogenic theory and geological practice, a host of large gold deposits (such as Sanshandao, Hexi, Fayunkuang) were successively discovered in the deep-seated structures (Li et al., 2013; Guo et al., 2017). The newly proven gold reserves have exceeded 2700 t, and the "stepped metallogenic model" is proposed (Goldfarb et al., 2001; Yang et al., 2003). However, the ore-controlling structure (Zhaoping fault and its secondary

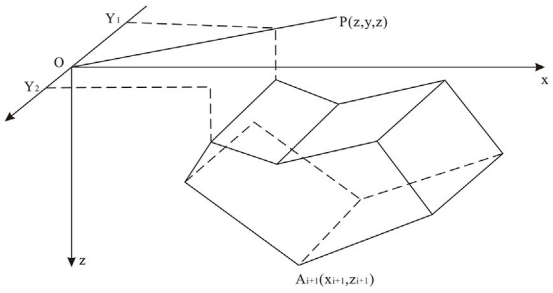

FIGURE 3
Schematic diagram of the two point five dimension level prism, modified after Fan et al., 2014.

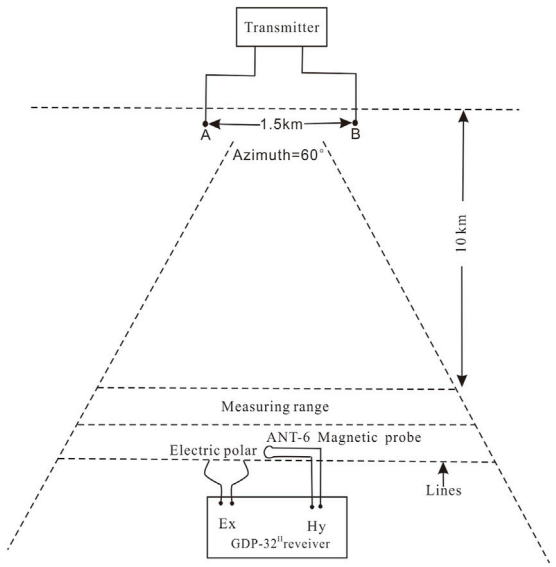

FIGURE 4
The CSAMT field observation system.

fault) of gold deposits is exposed sporadically (in Xiadian, Jiangjiayao gold deposits) beneath a thick cover of Quaternary basalts, which mean that only limited information can be obtained by traditional geological survey.

Here we present high-precision gravity and CSAMT methods to provide insights into spatial distribution of stratum, structure and magmatite for the Shanhou gold deposit hosting in southern part of Zhaoping fault. Moreover, relatively advanced data processing and inversion techniques help us to elucidate the coupling relationship between gold mineralized alteration zones and smooth-out waveform faults.

Geological setting

Regional geology

The Jiaodong gold province extends between the eastern NCC and northern SuLu metamorphic belt (Figure 1A) (Wei et al., 2001; Yang et al., 2016). It consists of Archean Jiaodong Group gneiss and Paleoproterozoic metamorphic sedimentary basement overlain by Proterozoic–Cenozoic carbonate rocks, volcano-sedimentary rocks, and loose sediment. The Late Jurassic Linglong granite, which are widespread in Jiaodong Peninsula and host large number of gold deposits. Geochronological results indicate that the formation age of granite was 166 ± 5.0 Ma (Figure 1B) (Yang et al., 2018; Deng et al., 2020). The middle Early Cretaceous Guojialing granite, which hosted several gold deposits, was emplaced between 133 and 126 Ma. The regional structures mainly consist of E-W- and NNE-NE-trending faults (Figure 1B) (Wang et al., 2014; Deng et al., 2020). The E-W-trending faults are mainly

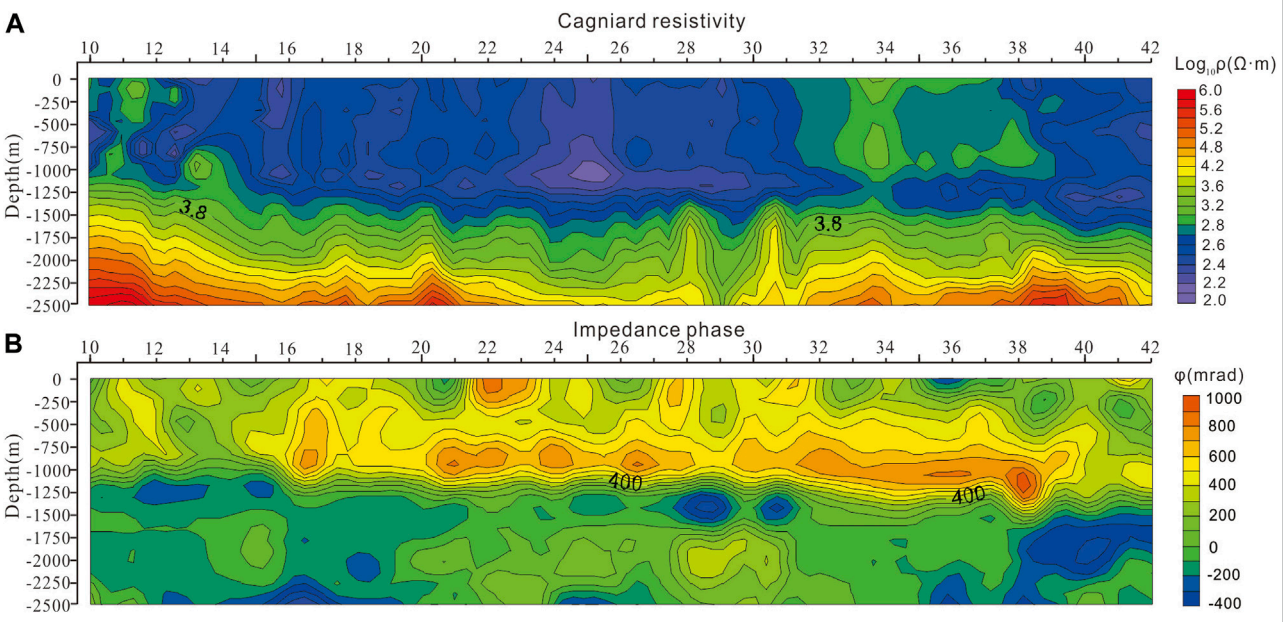

FIGURE 5
The pseudosection of the CSAMT profile; **(A)** Cagniard resistivity; **(B)** Impedance phase. The X-axis shows the survey point and the Y-axis shows the apparent depth.

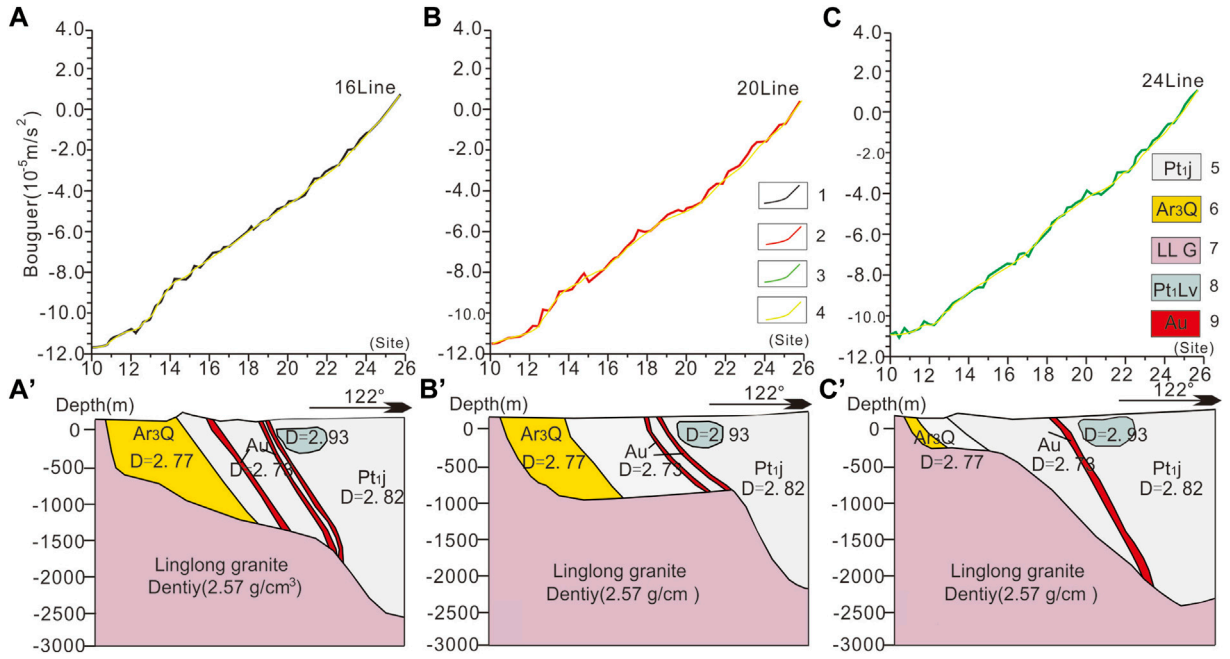

FIGURE 6
Man machine interactive inversion of three gravity profiles. **(A–C)** Observation curves and fitting curves; **(A′–C′)** Geologic interpretation. 1- Observation curve 16 line; 2- Observation curve 20 line; Observation curve 24 line; 4- Fitting curve; 5- Paleoproterozoic Jinshan Group; 6- Archean Qixia gneiss; 7-Late Jurassic Linglong granite; 8- Paleoproterozoic Lianzhou metabasite; 9- gold ore bodies.

metamorphic crystalline basement folds. The NNE-NE-trending ore-controlling faults are considered to be subparallel faults of the Tan-Lu fault. These ore-controlling faults are named Sanshandao, Jiaojia, Zhaoping, Xilin-douya, Jinniushan faults from west to east, respectively. The Zhaoping fault, for instance, with more than 1400 t of proven gold resources, directly controls the distribution of 17 large-scale gold deposits and 10 small-scale gold deposits (Yang et al., 2014).

Shanhou gold deposit is located in the southern part of the Zhaoping fault and is dominated by middle Early Cretaceous Guojialing granite, Archean Jiaodong Group gneiss, and Paleoproterozoic metamorphic rocks of the Jinshan Group (Figure 2). Three gold deposits (Xiadian, Beipo and Shanhou) are hosted in the granitic cataclastic rock and sericitized granitic cataclastic rock (Figure 2). Gold ore-bodies are typically controlled by brittle deformation structures, and show ductile-brittle deformation with sheared ores, altered rocks or pyrite aggregates, such as the elongated pyrite aggregates (Figure 2) (Yang et al., 2018).

TABLE 1 Density and specific resistivity data for the samples from the ore-bearing rocks and wall rocks in the Shanhou gold deposit.

Lithology	Number	Density	Specific resistivity
		Common value g/cm^3	Common value (Ω•m)
Paleoproterozoic Jinshan Group	23	2.82	4000
Linglong granite	30	2.57	8000
Archean Qixia gneiss	21	2.77	3000
Paleoproterozoic Lianzhou metabasite	6	2.93	7000
Ore-bearing rock	5	2.73	200

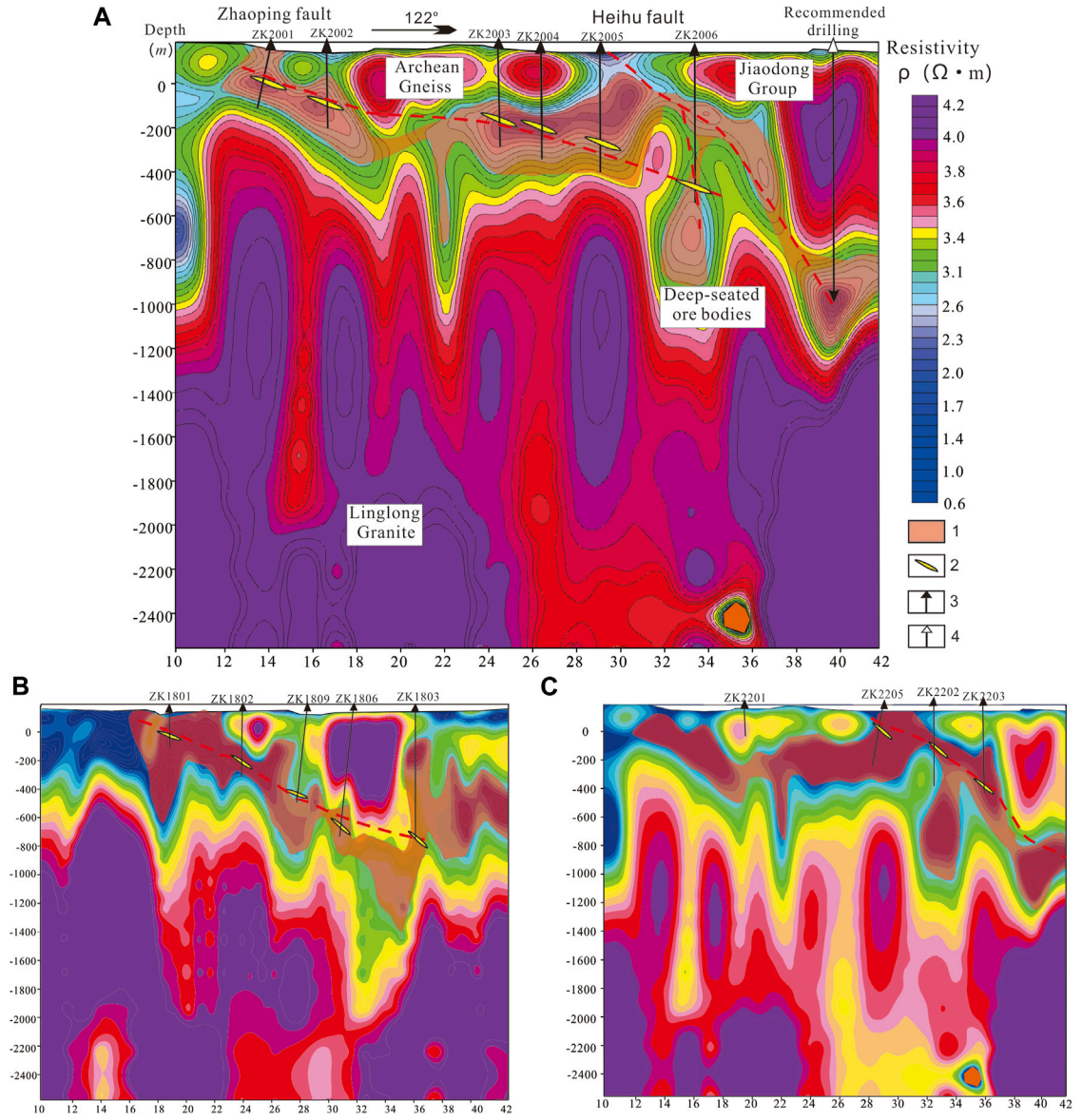

FIGURE 7
Inversion resistivity model of CSAMT by NLCG. **(A)** Line 20; **(B)** Line 18; **(C)** Line 22; 1- Ore-controlling brittle fracture; 2- The proven superficial gold bodies; 3- Drilled hole; 4- Recommended drilling.

Geophysical analytical techniques

Petrophysical parameters

Significant petrophysical parameters differences are the prerequisite of surveying geophysical research. Table 1 lists the petrophysical parameters in density and specific resistivity. The collected samples include the ore-bearing rocks and wall rocks in the Shanhou gold deposit. Samples from the Paleoproterozoic Jinshan Group yielded the relatively high density (2.82 g/cm^3) and high specific resistivity (4000 Ω m). The Linglong granite was characterized by low density (2.57 g/cm^3) and high specific resistivity (8000 Ω m), and the ore-bearing rocks by intermediate density (2.73 g/cm^3) and lowest specific resistivity (200 Ω m) (Table 1). This results are generally consistent with region petrophysical parameters statistics in Zhaoping fault (Xu et al., 2019).

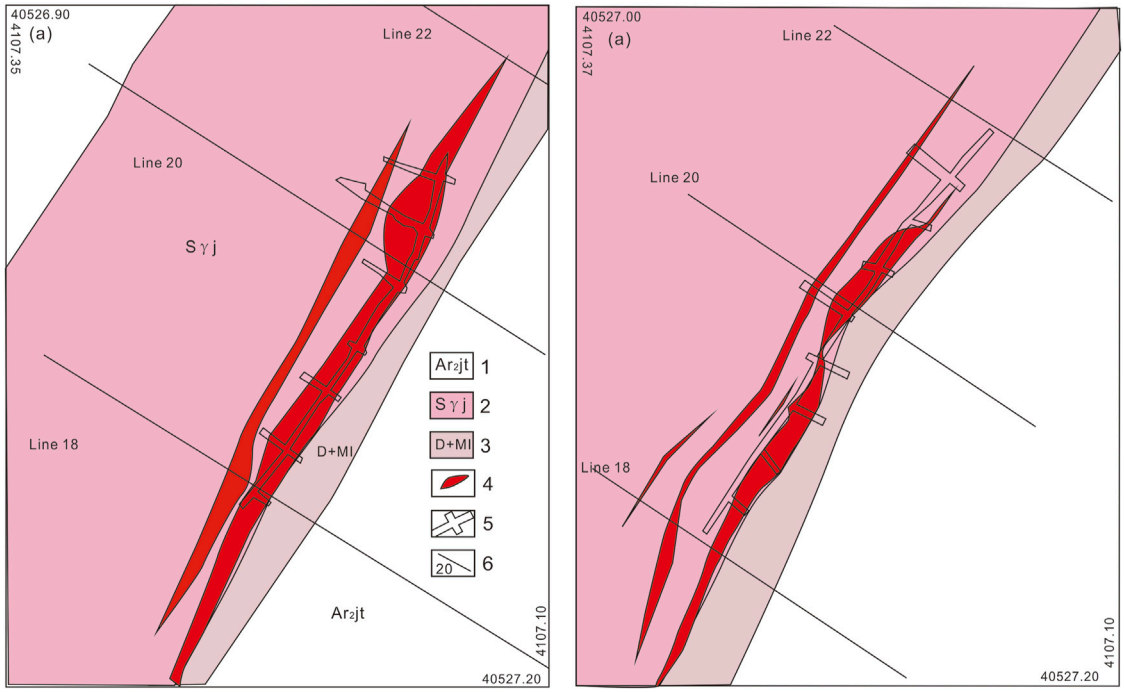

FIGURE 8
Geological map of tunnel samplings. **(A)** At the depth of –50 m; **(A)** At the depth of –100 m; 1- Archean plagioclase gneiss; 2- Sericitization granite; 3- Fault gouge and mylonite; 4- gold ore bodies; 5- tunnel; 6- geological profile.

High-precision gravity

Three high-precision gravimetric observation curves (Lines 16, 20 and 24) were collected along a section of 4.80 km long. These gravity profiles passes through the northeast–southwest–trending Zhaoping fault with the trend of NW. Each section included 33 continental gravity survey points at intervals of 50 m. It was collected by CG-5 type Gravimeter (Scintrex Corporation, Canada), which has the resolution less than 1 μGal, repeatability less than 5 μGal, and the static drift less than 0.02 mGal per day.

The two point five dimension man machine interactive inversion technology was applied to probe the deep-seated gold deposit (Figure 3). Firstly, the initial models are build according to the exiting gold metallogenic model. Then, the gravity forward modeling curves are subsequently calculated according to the initial models (Sui et al., 2004). The initial models were adjusted until the gravity forward modeling curves matching the field observation data (Yao et al., 1998). The gravity anomalies for any point, P (x, y, z), can be calculated using Eqs 1–5 (Yin et al., 2018) (Figure 3).

$$\Delta g(P) = G\sigma \sum_{i=1}^{N} \cos\varphi_i \left[I_i(Y_2) - I_i(Y_1) \right] \tag{1}$$

$$I_i(y) = y \ln \frac{u_{i+1} + R_{i+1}}{u_i + R_i} + u_{i+1} \ln(R_{i+1} + y) - u_i \ln(R_i + y) - w_i \left(\arctan \frac{u_{i+1} y}{w_i + R_{i+1}} - \arctan \frac{u_i y}{w_i R_i} \right) \tag{2}$$

$$u_i = x_i \cos\varphi_i + z_i \sin\varphi_i, u_{i+1} = x_{i+1} \cos\varphi_i + z_{i+1} \sin\varphi_i \tag{3}$$

$$R_i = \left(x_i^2 + y^2 + z_i^2 \right)^{1/2}, R_{i+1} = \left(x_{i+1}^2 + y^2 + z_{i+1}^2 \right)^{1/2} \tag{4}$$

$$\varphi_i = -x_i \sin\varphi_i + z_{i+1} \cos\varphi_i \tag{5}$$

where G, σ, and i are the gravitational constant, prism density, and prism corner number, respectively. The mean square error is about 7.20%.

Controlled source audio frequency magnetotellurics

CSAMT profile data were collected along a northwest–southeast-trending section of 3.10 km long (Figure 4). This section included 63 CSAMT survey points at intervals of 50 m. It was surveyed with broadband, multi-channel digital electromagnetic exploration system named GDP-32^{II} (Zonge Corporation, the United States of America). The GDP-32^{II} receiver is an 16-bit±1/2 low power consumption, high-accuracy data collected system, with one 250 mv/nT pass-band

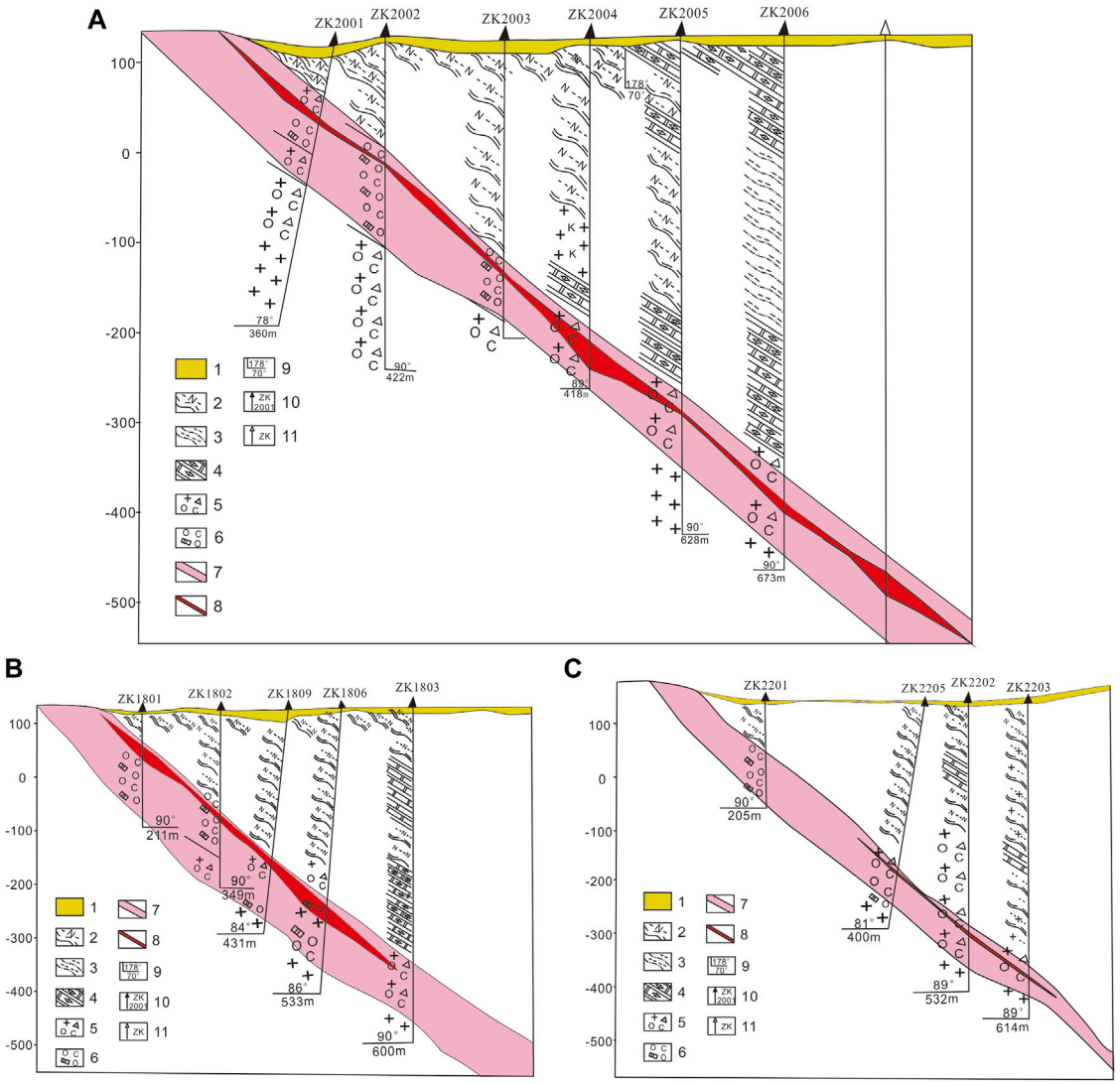

FIGURE 9
Geological profile of exploration in Shanhou gold deposit. **(A)** Line 20; **(B)** Line 18; **(C)** Line 22; 1- Quaternary; 2- Archean plagioclase gneiss; 3- Archean biotite granulite; 4- Paleoproterozoic dolomitic marble; 5- Sericitized cataclastic granite; 6- Pyrite sericite quartz; 7- Alteration zone; 8- gold bodies; 9- Occurrence $\frac{\text{inclination}}{\text{dip}}$; 10- Completed drilling; 11- Recommended drilling.

sensitivity ANT-6 senor, and 16 solid non-polarized poles for collecting electromagnetic signal instruments. The horizontal electric dipole transmitter was setting at E 120°18′12.02″, N 37°05′36.32″, and the emission current was about 30 A.

The results of smooth Cagniard resistivity and impedance phase indicate that the field survey data is true and effective (Figure 5). The commercial software gather the observed data and build a new model section, including line annotation, survey configuration, and inversion control. After multiple iterations, the initial inversion resistivity is obtain. Then the software automatically updates the model section and obtains the further inversion resistivity. Finally, the inversion errors (about 3.47%) satisfy the requirements (less than 7%).

Results

High-precision gravity

The amplitudes of high-precision gravity data are determined by two factors: lithology and fault. The overall trend of three gravity profiles are rising and degrading in some regional survey points. The black, red and green lines represent the field surveyed gravity curves. The yellow lines are the theoretical gravity curves which are calculated by two point five dimensional man-machine interactive inversion technology (Figures 6A–C). The assumed geological bodies were adjusted until the theoretical gravity curve is consistent with the measured gravity data (Yao et al., 1998).

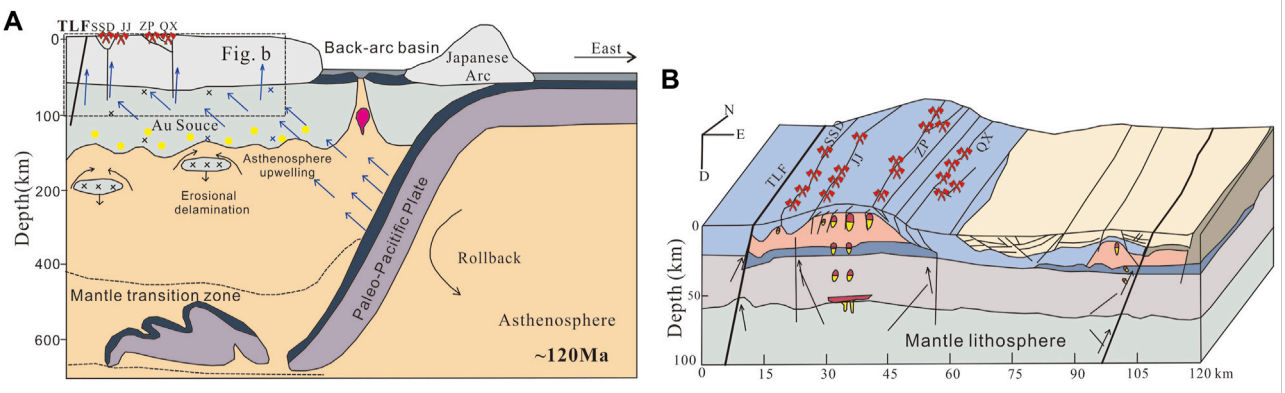

FIGURE 10
Cartoon showing the geodynamics of Jiaodong type gold deposit in Jiaodong gold province. **(A)** Metallogenic model of Jiaodong gold province; **(B)** Lithospheric and crustal architecture for the effective deposition of auriferous magma, modified from Deng et al. (2020).

According to the lithology exposed on the surface and regional petrophysical parameters, we conclude that the deeper subsurface geological body with the low value density (~2.57 g/cm^3) is consisted by the Late Jurassic Linglong granite. At shallow depth (top 1,000 m), between survey points 10 and 14, gravity profiles with an high density (~2.77 g/cm^3) should be corresponding to Archean Qixia gneiss. The intermediate to high gravity anomaly (~2.73 g/cm^3) likely corresponds to Zhaoping fault, which controls the distribution of Shanhou gold ore-bodies at survey points 16 and 18. The highest gravity anomaly (~2.82 g/cm^3), known as Paleoproterozoic Jinshan Group, lies in the southwestern part of Shanhou gold deposit, on one side of Zhaoping fault (Figures 6A'–C').

Controlled source audio frequency magnetotellurics profile

The CSAMT profile vertically passes through the trend of different geological bodies, producing a high resolution geoelectric structure (Figure 7). Laterally, two dimensional NLCG inversion results can be divided into three segments. The first one (sites 10–13) with intermediate to high apparent resistivity (~$10^{3.6}$ Ω m) should be corresponding to Late Jurassic Linglong granite. The second one (sites 15–28) with intermediate apparent resistivity (~$10^{3.2}$ Ω m) is the Archean gneisses. At survey point 14, an abrupt change in the apparent resistivity (10^4 to $10^{2.2}$ Ω m) is interpreted as a regional brittle fracture (named Zhaoping fault), which separates Linglong Granite from the Archean Qixia gneiss (Figure 7A). The third segment (sites 29–42) with highest apparent resistivity (~$10^{4.2}$ Ω m) is the Paleoproterozoic Jinshan Group. At survey point 28, Heihu fault with the low apparent resistivity (~$10^{2.2}$ Ω m) separates Archean Jiaodong Group from Paleoproterozoic Jinshan Group (Figure 7A).

Vertically, the inversion results can be segmented into three layers. The first layer (depths of 500 m) represents intermediate to high apparent resistivity ($10^{3.5}$–$10^{4.2}$ Ω m) geological bodies, including Late Jurassic Linglong granite, Archean Qixia gneiss and Paleoproterozoic Jinshan Group. The second layer (depths of 500–1000 m) with the lowest apparent resistivity (~$10^{2.0}$ Ω m) should be corresponding to deep-seated Zhaoping fault. This undulating fault no only controls the superficial Shanhou gold deposit, but also controls the deep-seated blind gold ore-bodies. According to the location of surface exposure and the apparent resistivity high value, the deeper layer should be consisted by Late Jurassic Linglong granite (Figure 7–9).

Discussion

Spatial correlation between gold mineralization and fault

The majority of Jiaodong type gold deposit, are characterized by massive gold ore bodies in deep-seated faults, such as Jiaodong Sanshandao gold deposit occurring in Sansandao fault, Liaodong Wulong gold deposit occurring in Jixingou fault, and Jilin Jiapigou gold deposit occurring in Jiapigou fault (Zhang et al., 2019; Zhang et al., 2020; Han et al., 2021).

The regional NNE-NE-trending faults in the Jiaodong gold province are regarded as the subsidiary fault of Tan-Lu fault. They are initially determined as the main gold ore-guided structures instead of the ore-controlling structures, such as Sanshandao, Jiaojia, Zhaoping, Qixia from west to east, respectively (Cox, 2010; Deng et al., 2019). Studies on the ore-forming fluid in above large gold belts indicated that the ore-forming fluid is basically consistent with the depths from deep to shallow domain (0 to −2,000 m) (Wu et al., 2022). Mineralization predictions in Jiaojia fault indicated that the occurring of gold

deposits in depth (−1700 to −1800 m) has great mineralization and a promising prospecting. However, Zhaoping fault is quite distinct from the other regional faults above with sporadically exposure. Therefore, the deep mineral prospecting has still faced a downturn.

Geodynamics of Jiaodong type gold deposit in Jiaodong gold province

Tectonic altered rock type or dissemination type gold deposits are commonly coupling with NNE-NE trending brittle faults, which are sub-parallel to the Tan-Lu fault to the west (Deng et al., 2015). Geological and geophysical results reveal that the Shanhou gold deposits are generally hosting in the footwall of the faults within Linglong Granite. The clustered gold deposits distributed in the smooth-out waveform faults indicated that Zhaoping fault has experienced transpression and extension (Deng et al., 2015, Deng et al., 2019). The development of strike-slip motion was triggered by the transition from transpression to transtension and then the gold ore-bodies with industrial grade deposited in the gentler-dipping parts of these NNE-NE trending faults. Thus, the lithospheric-scale Tan-Lu fault is the first-order architectural control on the Jiaodong Peninsula. This lithospheric-scale fault plays a role of connection between lithosphere and crust for its secondary parallel faults.

At plate tectonic scale, the Paleo-Pacific Plate had a slow northwesterly subduction earlier than ~135 Ma and then gradually deflected in a clockwise direction during 135–125 Ma. At the period of 125–100 Ma, the abrupt breakoff and roll-back of the subduction slab triggered the destruction of NCC, resulted in extension and thinning of lithosphere (Deng et al., 2015; Zhu et al., 2015; Liang et al., 2019; Wu et al., 2022). Within the Jiaodong gold province, the far-field stresses of subduction produced the development of lithosphere-scale Tan-Lu fault and its second-order faults (Figure 10A) (Deng et al., 2020).

The far-field stresses of subduction of Paleo-Pacific Plate triggered the temporal evolution of igneous activity and the structural geometries of gold deposits (Zhu and Sun, 2021). Thus, the Zhaoping fault can rapidly migrate the sub-crustal auriferous fluid without forming extensive melts and control the distribution of gold deposits, such as Jiangjiayao, Xiadian, Shanhou, and Shiqiao gold deposits (Figure 10B). The mineralization of Jiaodong type gold deposits was commonly related to subduction of Paleo-Pacific Plate (Deng et al., 2015).

Conclusion

1) Based on the results of the high-precision gravity and CSAMT profiles, smooth-out waveform geophysical anomaly regarded as ore-bearing zone was identified.
2) The smooth-out waveform fault is essential to the effective deposition of auriferous magma.
3) The mineralization of Jiaodong type gold deposits was commonly related to subduction of Paleo-Pacific Plate.

Data availability statement

The original contributions presented in the study are included in the article/Supplementary Material, further inquiries can be directed to the corresponding authors.

Author contributions

Z-HX designed the surveys and carried them out. G-WG performed the geophysical data processing. Z-JD and G-WG performed the geophysical data processing. J-YJ, LW, and X-GN prepared the manuscript with contributions from all co-authors. Z-JD prepared the manuscript with contributions from all co-authors.

Funding

This research benefited from the support of Fundamental Research Funds for the Central Universities (ZY2299211143), Shandong Provincial Engineering Laboratory of Application and Development of Big Data for Deep Gold Exploration Funds (SDK202221), and Science and Technology Research Project in Higher Learning Institutions of Hebei Province (ZC2022106), and Engineering Research Center of Geothermal Resources Development Technology and Engineering (22006).

Acknowledgments

We thank Frontiers in Earth Science Topic Editors for their critical reviews of an earlier version of this paper, which helped us to improve the quality. We thank Jilin University Fengyue Sun, LW and Jilin Exploration Geophysics Institute Chief Engineer Fuwen Li for their helpful suggestions during manuscript preparation, This research has been funded by the Engineering Research Center of Geothermal Resources DevelopmentTechnology and Engineering, Ministry of Education, Jilin University.

Conflict of interest

Author X-GN was employed by Inner Mongolia Non-ferrous Geological Mining Industry.

The remaining authors declare that the research was conducted in the absence of any commercial or financial relationships that could be construed as a potential conflict of interest.

Publisher's note

References

Cai, Y. C., Fan, H. R., Santosh, M., Hu, F. F., Yang, K. F., and Li, X. H. (2018). Decratonic gold mineralization: Evidence from the Shangzhuang gold deposit, eastern North China Craton. *Gondwana Res.* 54, 1–22. doi:10.1016/j.gr.2017.09.009

Cox, S. F. (2010). The application of failure mode diagrams for exploring the roles of fluid pressure and stress states in controlling styles of fracture-controlled permeability enhancement in faults and shear zones. *Geofluids* 10, 217–233. doi:10.1111/j.1468-8123.2010.00281.x

Deng, J., Wang, C. M., Bagas, L., Carranza, E. J. M., and Lu, Y. (2015). Cretaceous–cenozoic tectonic history of the Jiaojia fault and gold mineralization in the Jiaodong Peninsula, China: Constraints from zircon U–Pb, illite K–Ar, and apatite fission track thermochronometry. *Min. Depos.* 50, 987–1006. doi:10.1007/s00126-015-0584-1

Deng, J., Yang, L. Q., Groves, D. I., Zhang, L., Qiu, K. F., and Wang, Q. F. (2020). An integrated mineral system model for the gold deposits of the giant Jiaodong province, eastern China. *Earth-Science Rev.* 208 (2), 103274. doi:10.1016/j.earscirev.2020.103274

Deng, J., Yang, L. Q., Li, R. H., Groves, D. I., Santosh, M., Wang, Z. L., et al. (2019). Regional structural control on the distribution of world class gold deposits: An overview from the giant Jiaodong gold province, China. *Geol. J.* 54, 378–391. doi:10.1002/gj.3186

Fan, Z. G., Huang, X. Z., Tan, L., Yang, X., Zhang, H., Zhou, D., et al. (2014). A study of iron deposits in the Anshan area, China based on interactive inversion technique of gravity and magnetic anomalies. *Ore Geol. Rev.* 57, 618–627. doi:10.1016/j.oregeorev.2013.09.017

Goldfarb, R., Groves, D. I., and Gardoll, S. (2001). Orogenic gold and geologic time: A global synthesis. *Ore Geol. Rev.* 18, 1–75. doi:10.1016/s0169-1368(01)00016-6

Groves, D. I., and Bierlein, F. P. (2007). Geodynamic settings of mineral deposit systems. *J. Geol. Soc. Lond.* 164, 19–30. doi:10.1144/0016-76492006-065

Groves, D. I., Santosh, M., and Zhang, L. (2020). A scale-integrated exploration model for orogenic gold deposits based on a mineral system approach. *Geosci. Front.* 11 (3), 719–738. doi:10.1016/j.gsf.2019.12.007

Groves, D. I., Vielreicher, R. M., Goldfarb, R. J., and Condie, K. C. (2005). Controls on the heterogeneous distribution of mineral deposits through time. *Geol. Soc. Lond. Spec. Publ.* 248 (1), 71–101. doi:10.1144/gsl.sp.2005.248.01.04

Guo, L. N., Goldfarb, R. J., Wang, Z. L., Li, R. H., Chen, B. H., and Li, J. L. (2017). A comparison of jiaojia-and linglong-type gold deposit ore-forming fluids: Do they differ? *Ore Geol. Rev.* 88, 511–533. doi:10.1016/j.oregeorev.2016.12.003

Han, J. L., Deng, J., Zhang, Y., Sun, J., Wang, Q., Zhang, Y., et al. (2021). Au mineralization-related magmatism in the giant Jiapigou mining district of Northeast China. *Ore Geol. Rev.* 141, 104638. doi:10.1016/j.oregeorev.2021.104638

Li, C., Li, L., Li, C. R., Santosh, M., and Shen, J. F. (2022). Geochemistry of hydrothermal zircon as a proxy to fingerprint ore fluids in late Mesozoic decratonic gold deposits. *Ore Geol. Rev.* 143, 104703. doi:10.1016/j.oregeorev.2022.104703

Li, J., W., Bi, S. J., Selby, D., Chen, L., Vasconcelos, P., Thiede, D., et al. (2012). Giant Mesozoic gold provinces related to the destruction of the North China craton. *Earth Planet. Sci. Lett.* 349-350, 26–37. doi:10.1016/j.epsl.2012.06.058

Li, X. C., Fan, H. R., Santosh, M., Hu, F. F., Yang, K. F., and Lan, T. G. (2013). Hydrothermal alteration associated with Mesozoic granite-hosted gold mineralization at the Sanshandao deposit, Jiaodong Gold Province, China. *Ore Geol. Rev.* 53, 403–421. doi:10.1016/j.oregeorev.2013.01.020

Liang, Y. Y., Deng, J., Liu, X., Wang, Q., Ma, Y., Gao, T., et al. (2019). Water contents of early cretaceous mafic dikes in the Jiaodong Peninsula, eastern north China craton: Insights into an enriched lithospheric mantle source metasomatized by paleo–Pacific plate subduction–related fluids. *J. Geol.* 127 (3), 343–362. doi:10.1086/702648

Sui, S. W., Yu, C. C., and Yao, C. L. (2004). The semi-intelligent processing and interpretation software for gravity and magnetic anomalies along the profile of rolling topography and its application. *Geophys. Geochem. Explor.* 28 (1), 65–68. doi:10.3969/j.issn.1000-8918.2004.01.017

Wang, Z. L., Yang, L. Q., Deng, J., Santosh, M., Zhang, H. F., Liu, Y., et al. (2014). Gold-hosting high Ba-Sr granitoids in the Xincheng gold deposit, Jiaodong Peninsula, East China: Petrogenesis and tectonic setting. *J. Asian Earth Sci.* 95, 274–299. doi:10.1016/j.jseaes.2014.03.001

Wei, W. S., Mu, T., and Zhang, H. H. (2001). *Geological map of Jiaodong gold Province showing the metallogenic belts, ore deposit types and distribution of the gold deposits*. Lang Fang, Hebei: Gold Geology Research Institute of China Armed Police Force.

Wu, J. J., Zeng, Q. D., Santosh, M., Fan, H., Bai, R., Li, X., et al. (2022). Deep ore-forming fluid characteristics of the Jiaodong gold province: Evidence from the Qianchen gold deposit in the Jiaojia gold belt. *Ore Geol. Rev.* 145, 104911. doi:10.1016/j.oregeorev.2022.104911

Xu, Z. H., Sun, F., Xin, W., Sun, N., Li, F., Niu, J., et al. (2019). formation and evolution of paleoproterozoic orogenic belt in southern Jilin, jiao–liao–ji belt, north China craton: Constraints from Geophysics. *Precambrian Res.* 333, 105433. doi:10.1016/j.precamres.2019.105433

Yang, J. H., Wu, F. Y., and Wilde, S. A. (2003). A review of the geodynamic setting of large-scale Late Mesozoic gold mineralization in the North China Craton: An association with lithospheric thinning. *Ore Geol. Rev.* 23, 125–152. doi:10.1016/s0169-1368(03)00033-7

Yang, L. Q., Deng, J., Wang, Z. L., Guo, L. N., Li, R. H., Groves, D. I., et al. (2016). Relationships between gold and pyrite at the xincheng gold deposit, Jiaodong Peninsula, China: Implications for gold source and deposition in a brittle epizonal environment. *Econ. Geol.* 111, 105–126. doi:10.2113/econgeo.111.1.105

Yang, L. Q., Dilek, Y., Wan, Z. L., Weinberg, R. F., and Liu, Y. (2018). Late jurassic, high Ba–Sr Linglong granites in the Jiaodong Peninsula, east China: Lower crustal melting products in the eastern north China craton. *Geol. Mag.* 155, 1040–1062. doi:10.1017/s0016756816001230

Yao, C. L., Li, Y. S., and Guan, Z. N. (1998). Improvement of real-time and visualized forward and inversion of gravity andmagnetic anomalies. *Geoscience* 12 (1), 115–122.

Yin, J. N., Lindsay, M., and Teng, S. R. (2018). Mineral prospectivity analysis for BIF iron deposits: A case study in the Anshan-Benxi area, Liaoning province, North-East China. *Ore Geol. Rev.* 120, 102746. doi:10.1016/j.oregeorev.2018.11.019

Zhang, L., Groves, D. I., Yang, L. Q., Wang, G. W., Liu, X. D., Li, D. P., et al. (2020). Relative roles of formation and preservation on gold endowment along the Sanshandao gold belt in the Jiaodong gold province, China: Importance for province- to district-scale gold exploration. *Min. Depos.* 55 (2), 325–344. doi:10.1007/s00126-019-00908-1

Zhang, Z., Wang, G., Carranza, E., Zhang, J., Tao, G., Zeng, Q., et al. (2019). Metallogenic model of the Wulong gold district, China, and associated assessment of exploration criteria based on multi-scale geoscience datasets. *Ore Geol. Rev.* 114, 103138. doi:10.1016/j.oregeorev.2019.103138

Zhu, R., and Sun, W. (2021). The big mantle wedge and decratonic gold deposits. *Sci. China Earth Sci.* 64 (9), 1451–1462. doi:10.1007/s11430-020-9733-1

Zhu, R. X., Chen, L., Wu, F. Y., and Liu, J. (2011). Timing, scale and mechanism of the destruction of the North China Craton. *Sci. China Earth Sci.* 547, 789–797. doi:10.1007/s11430-011-4203-4

Zhu, R. X., Fan, H. R., Li, J. W., Meng, Q., Li, S., and Zeng, Q. (2015). Decratonic gold deposits. *Sci. China Earth Sci.* 58, 1523–1537. doi:10.1007/s11430-015-5139-x